Swiss J Geosci (2013) 106:491–504
DOI 10.1007/s00015-013-0147-3

K-feldspar rich shales from Jurassic bedded cherts in southeastern Slovenia

Simona Skobe · Špela Goričan · Dragomir Skaberne · Tomaž Verbič · Miha Mišič · Nina Zupančič

Received: 15 March 2013 / Accepted: 10 September 2013 / Published online: 26 October 2013

Abstract The study area in southeastern Slovenia is part of the transitional zone between the internal and the external Dinarides. Within Jurassic bedded cherts there are up to 2 cm thick shale intercalations, consisting of laminated, soft, fine-grained, green to brown material whose origin has been in question. In the majority of Tethyan cherts, the interbedded material is reported to be volcanogenic and/or terrigenous, although a detailed mineralogical analysis of the material is lacking. An XRD analysis confirmed the presence of quartz, illite, chlorite and K-feldspar, which is the prevailing component in some samples. Major and trace element data exclude both a volcanogenic and an hydrothermal origin. Several discrimination diagrams indicate the upper crustal terrigenous nature of shales and a biogenic silica source. The source material was probably from a Variscan crust, which at the time of deposition had already been weathered to kaolinite, and some sporadic muscovite. The MnO/Al_2O_3 ratio suggests a slow sedimentation rate of cherts and a faster one for shales, which probably settled from distal turbidity currents. The negative Ce anomaly indicates prolonged contact with ocean water. Sediments were deposited on a Tethyan passive margin, originally as silica-rich carbonate beds intercalated with mud. During late diagenesis, the mixing of marine and meteoric waters caused the further silicification of limestone and simultaneous potassium enrichment of shale which led to their alteration into illite or chlorite and, in sediments already rich in K-minerals, into K-feldspar.

Keywords Dinarides · Tethyan cherts · Geochemistry · Diagenesis · Silicification · Discrimination diagrams

Editorial handling: W. Winkler & A. G. Milnes.

S. Skobe · N. Zupančič (✉)
Department of Geology, Faculty of Natural Sciences and Engineering, University of Ljubljana, Aškerčeva 12, 1000 Ljubljana, Slovenia
e-mail: nina.zupancic@ntf.uni-lj.si

S. Skobe
e-mail: simona.skobe@ntf.uni-lj.si

Š. Goričan · N. Zupančič
Ivan Rakovec Institute of Palaeontology, ZRC SAZU, Novi trg 2, 1000 Ljubljana, Slovenia
e-mail: spela@zrc-sazu.si

D. Skaberne · M. Mišič
Geological Survey of Slovenia, Dimičeva ulica 14, 1000 Ljubljana, Slovenia
e-mail: dragomir.skaberne@geo-zs.si

M. Mišič
e-mail: miha.misic@yahoo.com

T. Verbič
Arhej d.o.o., Rimska 1, 1000 Ljubljana, Slovenia
e-mail: tomazver@gmail.com

1 Introduction

The study area is part of the transitional zone between the External and the Internal Dinarides (Fig. 1; see Placer 1999). In terms of palaeogeography, this zone corresponds to the proximal continental margin of the Adriatic plate, more specifically, to the transition between the Dinaric Carbonate Platform (also called the Adriatic Carbonate Platform) and the deep-water Slovenian Basin. The stratigraphic succession is characterised by Triassic to Lower Jurassic shallow-water carbonates overlain by Middle Jurassic to Upper Cretaceous basinal deposits. The Jurassic pelagic rocks (Izvir Formation of Rižnar 2005) are cherts

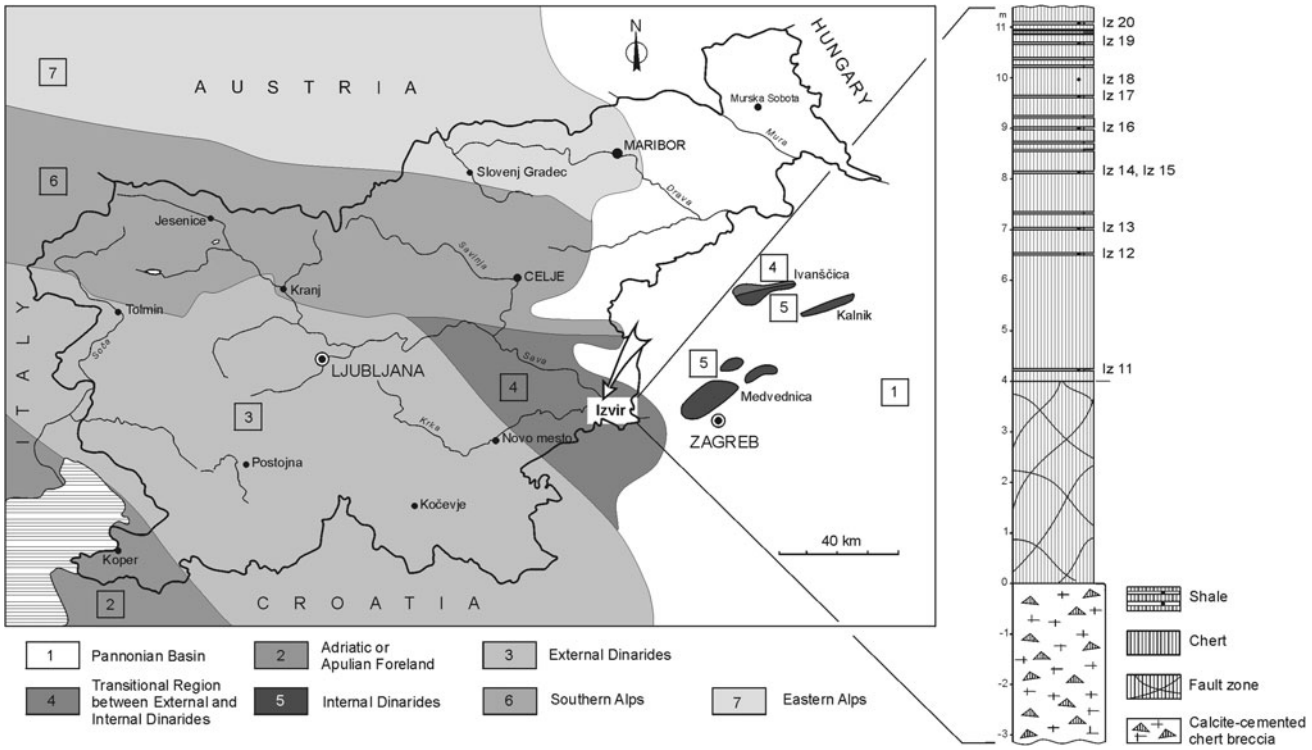

Fig. 1 Location map and stratigraphic log of the Izvir section with the position of the samples (tectonic subdivision simplified according to Placer 1999)

interbedded with thin greenish fine-grained beds (Fig. 1). These beds could have either a volcanogenic or terrigenous origin. Interpretations of the palaeoenvironment and palaeogeographic position of the area in the Tethys realm are very important for determining the origin of the interbedded material.

Bedded cherts are the most common Middle and Upper Jurassic pelagic sediments of the entire Tethys (for review, see Baumgartner 2013). They occur in deep-water Tethyan basins, including those preserved in the Dinarides, Southern Alps and Apennines. The stratigraphy of these cherts has been studied extensively but provenance studies of the non-biogenic components are rare (Barrett 1981; Baltuck 1982; Amodeo 1999; Di Leo et al. 2002a, b; Halamić et al. 2005; Peh and Halamić 2010). In the majority of Jurassic and also Triassic cherts, the interbedded material is reported to be volcanogenic and/or terrigenous, although a detailed analysis of the material is lacking, since the research focus has been on the cherts. In northwestern Croatia, in close proximity to the study area, intercalations of volcanic origin have been proven beyond doubt only in Triassic sequences; tuffitic interlayers occur in the successions of the continental margin (Mts. Žumberak and Ivanščica) and back-arc basin (Mts. Medvednica and Kalnik; see Halamić et al. 2001). In contrast, Middle Jurassic radiolarites of the same area alternate with shales, silicified shales, siltites or matrix-supported conglomerates that formed in an accretionary wedge and seem to be devoid of tuffitic material (Halamić et al. 1999, 2005). Nevertheless, the potential volcanic origin of the greenish fine-grained beds at Izvir must be considered because ample evidence for Jurassic volcanism exists in the broader region. For example, from the carbonate platform succession in western Croatia (Mt. Velika Kapela), a Kimmeridgian to Lower Tithonian deeper-water interval with thin beds of cherts and thin interbeds of tuffs to tuffitic mudstones has been reported (Velić et al. 2002). Further south, in Middle Dalmatia, the correlative Lemeš beds include layers of bentonite that are several metres thick (Braun 1991). Thinner bentonite layers also occur in the Rosso Ammonitico Veronese of the Southern Alps in northern Italy (Bernoulli and Peters 1970); these are assigned to the Middle Oxfordian to possibly Lower Kimmeridgian (Baumgartner et al. 1995b; Beccaro 2006). In the Italian Apennines, in the lower part of the *Scisti silicei* Formation (upper Triassic–Jurassic), the volcanoclastic layers are similar to arc-related rhyolitic tephra in a subaqueous environment (Di Leo et al. 2002b).

The aim of the present paper is to describe the mineralogical and geochemical characteristics of the interbedded material in the Jurassic bedded chert sequences, to establish its provenance and depositional environment, and to compare it with similar rocks from neighbouring areas. It is

hoped that the results will contribute to a better understanding of the geochemical control of the sedimentary evolution of the Jurassic bedded cherts in Tethys palaeomargin.

2 Geological setting

In an abandoned quarry (long 15° 32′ 52.2″ E; lat 45° 51′ 34.7″ N, in the WGS84 coordinate system) near the village of Izvir on the southern rim of the Krško depression, on the slopes of the Gorjanci Mountains (Fig. 1), Jurassic cherts are interbedded with greenish fine-grained material.

According to Rižnar (2005), the area is part of a transitional zone formed by the rifting of a thinned (micro)continental margin on which, due to rapid subsidence, pelagic sediments were deposited. The sedimentary rocks of deep-water facies are divided into five formations from the Middle or Upper Jurassic to the end of the Cretaceous (Rižnar 2005). The Izvir Formation is the oldest (?Middle, Upper Jurassic) of the Šutna Group. Its lower limit is defined by cherts (Rižnar 2005) which are absent in platform rocks of the Rhaetian to Lower Jurassic. The Izvir Formation is conformably overlain by the Biancone formation of grey micritic limestone with chert nodules and beds, thin-bedded yellowish micritic limestone with chert and marly limestone, and carbonate breccia with laminae of yellowish marl. The age of the Biancone formation is from Late Tithonian to Valanginian, possibly to Hauterivian-Barremian (Rižnar 2005). The overall Jurassic and Cretaceous stratigraphy is typical of subsided Tethyan continental margins. Bedded radiolarian chert as predominant Middle and Upper Jurassic facies and the overlying Biancone (or Maiolica) cherty limestone are characteristic of normal pelagic sedimentation on these margins (for a recent review, see Baumgartner 2013).

The studied alternation of chert and shale (the Izvir Formation) accumulated in the marginal parts of the Slovenian Basin. The depositional area was located close to the Dinaric Carbonate Platform (now the External Dinarides, see Fig. 1) that occupied the most stable proximal part of the Adriatic continental margin facing the Neotethys (for a broader palaeogeographic picture see Fig. 2b in Schmid et al. 2008). The distal continental-margin units as well as the ophiolitic mélange units are now part of the Internal Dinarides exposed in inselbergs east of the study area (Fig. 1). The ophiolitic mélange of these inselbergs belongs to the Western Vardar Ophiolitic Unit (see Plate 1 in Schmid et al. 2008). The present-day position of the Western Vardar Ophiolitic Unit in close vicinity to the proximal continental-margin units (Fig. 1) can be explained by the considerable westward displacement of the ophiolites during the Cretaceous to Cenozoic out-of-sequence thrusting that followed their obduction in the Late Jurassic (see Schmid et al. 2008 and the references therein).

3 Materials and methods

3.1 Description of the studied section

The examined section is composed of two separate parts, which partially overlap. The basal part of the succession comprises crystalline late diagenetic dolomite of Late Triassic age. Its colour is constant light grey (2.5Y7/1 and 10YR7/2). Above the dolomite there is an angular unconformity, which has regional significance. The unconformity was produced by extensional tectonics linked to the break-up of the carbonate platform and a distinctive change in the sedimentary environment.

The dolomite is covered by coarse-grained calcite-cemented chert breccias (lower part of the stratigraphic column shown in Fig. 1). The chert clasts are predominately very angular and up to 0.3 m in diameter, and in places some smaller limestone clasts occur. They are bound by xeno- to hipidiotopic sparite that replaces the former intrapelmicritic matrix of the breccias (Fig. 2a). The dolomite partly replaces chert clasts too (Fig. 2a, b). The thickness of the breccia is more than 3 m, but the full thickness is impossible to measure directly due to incomplete local exposure. Based on rare outcrops, the thickness probably reaches up to 20 m. At the examined section the breccia is cut by a minor fault which has a strike-slip and normal component. The fault zone is 2–4 m thick and consists of angular blocks of breccia and chert floating in a poorly lithified (sandy and muddy) fine-grained matrix. The fault zone dips steeply towards NW.

Above the fault zone there is a vitreous chert with a bed thickness of 5–25 cm with very thin muddy intercalations, only up to a few mm in thickness. These beds have the same orientation as the fault zone; they dip steeply towards NW and almost reach a vertical position in the upper part of the exposed sequence. The colour of the chert varies from grey (5Y6/1) to olive brown (2.5Y4/3), to dark yellowish brown (10YR3/4) and almost black (5Y2.5/2). Typically, chert is speckled throughout the sequence. According to its texture, it seems that it was formed by silicification of a siliceous biopelmicritic limestone (Fig. 2c). In some places, lamination is amplified by a variable degree of silicification (Fig. 2d). The chert consists mostly of microquartz and chalcedonic quartz with some crystals of pyrite which are mostly oxidised (Fig. 2e, f). Mega-quartz is very subordinate. The chert is cut by thin veins and fractures of different generations. The veins are filled by chalcedonic, micro-, and mega-quartz (Fig. 2g) and calcite. Calcite and dolomite partly replace all quartz

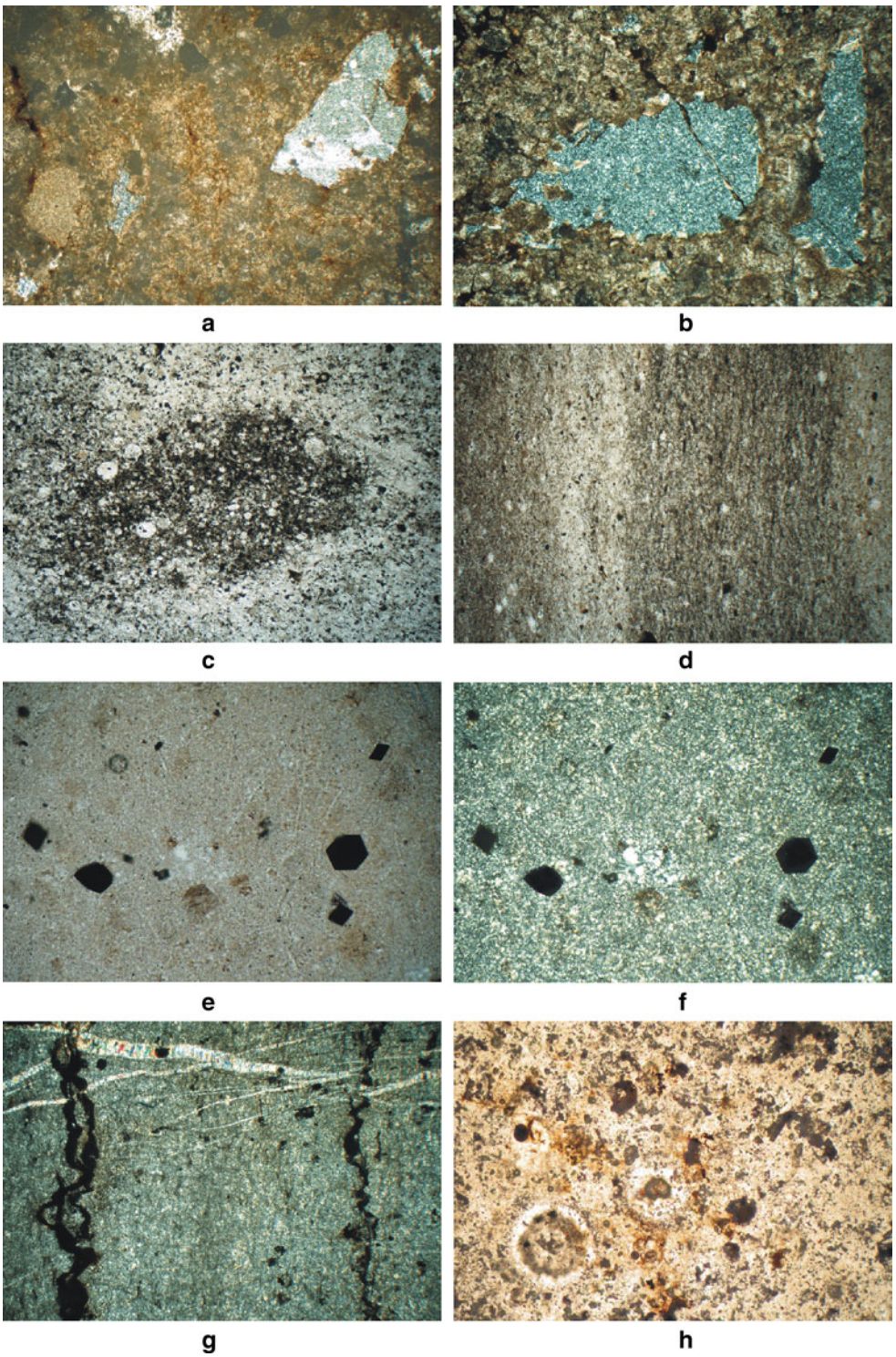

Fig. 2 The calcite-cemented chert breccia: **a** angular chert clasts and smaller microsparitic clasts in predominantly xenotopic sparite with relicts of a not completely replaced and recrystallised intrapelmicritic matrix (XPL: LA 4.4 mm). **b** The chert clasts partly replaced by calcite in xeno- to hipidiotopic sparite (XPL: LA 2.34 mm). **c** The chert: inclusion of less silicified biomicrite with radiolarians and opaque minerals (pyrite) in microquartz with small inclusions of not completely replaced biomicrite (PPL: LA 4.4 mm). **d** Lamination in the chert amplified by different degrees of silicification and inclusions of not completely replaced limestone with radiolarians, sponge spicules and opaque minerals (pyrite) in *darker* laminae (PPL: LA 4.4 mm). **e** Chert—microquartz with radiolarians, sponge spicules, euhedral crystals of pyrite and dolomite replacing microquartz (PPL: LA 1.17 mm). **f** Same as **e** (XPL: LA 1.17 mm). **g** Chert laminae in stylolitic contact enriched with opaque minerals cut by veins filled by elongated mega- and microquartz (XPL: LA 4.4 mm). **h** Chert—microquartz with inclusions of not completely replaced limestone with oxidised pyrite, radiolarians and some euhedral crystals of dolomite replacing microquartz (PPL: LA 1.17 mm). Key: *PPL* plane-polarised light, *XPL* cross-polarised light, *LA* longer photo axis

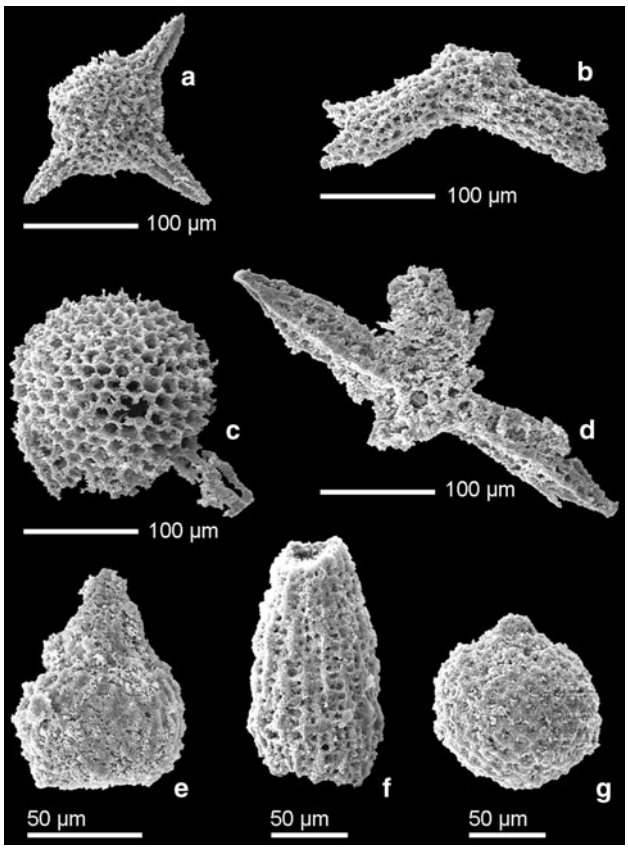

Fig. 3 Radiolarians from sample Iz 18. **a** *Haliodictya*? *hojnosi* Riedel and Sanfilippo, **b** *Paronaella* sp., **c** *Triactoma* sp., **d** *Tetraditryma corralitosensis* (Pessagno), **e** *Eucyrtidiellum nodosum* Wakita, **f** *Transhsuum* cf. *maxwelli* (Pessagno), **g** *Hemicryptocapsa* cf. *yaoi* (Kozur)

varieties. Stylolites (Fig. 2g) and an elliptic cross-section of radiolarians as products of pressure solution processes were detected in places. Remains of radiolarians and sponge spicules (Fig. 2c–f, h) were found in all samples.

The preservation of fossils is very poor but a few radiolarian taxa could be identified. *Eucyrtidiellum nodosum* Wakita, *Haliodictya*? *hojnosi* Riedel and Sanfilippo, and *Tetraditryma corralitosensis* (Pessagno) in sample Iz18 (Fig. 3) allow a broad age assignment to the Bajocian to early Kimmeridgian (Unitary Association Zones 3 to 10 of Baumgartner et al. 1995a).

The colour of the intercalations varies from greyish olive (10Y4/2) to pale green (10G6/2) when not affected by oxidation. The intercalations gradually become thicker and reach a thickness of up to 50 mm, whereas the chert beds become thinner in the uppermost part of the exposed sequence (Fig. 1). The thickness of the complete sequence could not be measured due to the incomplete exposure. The sequence (Izvir formation) is overlain by platy limestone with chert nodules and lenses, informally known as the Biancone formation. The contact between the two formations is nowhere exposed. Based on the rare exposures, the complete thickness of the chert sequence probably lies between 70 and 120 m.

Table 1 Field description and mineralogical composition of the Izvir samples

	Quartz	Muscovite/ illite	Chlorite	K-fs	Pl
Iz11					
First several mm thick laminated muddy intercalation	23	67	6		4
Iz12					
Second several mm thick muddy intercalation	33	53	14		
Iz13					
Third several mm thick muddy intercalation	26	61	13		
Iz14					
Fourth 2–3 cm muddy intercalation of fine-grained hard brown porous material	3			97	
Iz15					
Same layer as Iz14, except that the material is soft	24	26	40	10	
Iz16					
1–5 cm thick bed of sandstone-like chert between vitreous chert layers	90	10			
Iz17					
Several cm thick muddy intercalation from upper part of profile	26	34	16	24	
Iz18					
Chert	100				
Iz19					
Brown coloured muddy intercalation from upper part of profile	41	30	22	7	
Iz20					
Uppermost white coloured muddy intercalation	8	19	19	54	

A semi-quantitative estimation in % of the bulk sample and clay mineralogical compositions was calculated using data from Schultz (1964), Mišič (1998) and Moore and Reynolds (1997)

3.2 Samples and methods

Because a preliminary sample set of the intercalated shales revealed high K-feldspar contents, a further suite of 10 samples was systematically analysed (Fig. 1, samples Iz11–Iz20). The characteristics of the samples are shown in Table 1.

The mineralogical composition of all the samples were established by powder X-ray diffraction. The samples were pulverised by hand in an agate mortar and pressed into an aluminium holder. XRD measurements were conducted using a Philips PW 3830 diffractometer equipped with CuKα radiation and a graphite monochromator. The X-ray radiation was generated at a voltage of 40 kV and a current of 30 mA. Data were recorded in the range $2° \leq 2\Theta \leq 70°$. A semi-quantitative estimation of the bulk sample and clay mineralogical composition was calculated using data from Schultz (1964), Mišič (1998) and Moore and Reynolds (1997).

The chemical compositions of 11 samples, samples Iz11–Iz20 together with one analytical replicate (Iz20r), were measured by ACME Analytical Laboratories in Canada. A classical whole-rock analysis for major oxides and several minor elements, rare earths and refractory elements was carried out by ICP–ES (Inductively Coupled Plasma-Emission Spectrometry) following a lithium borate fusion to give total abundances. Precious metals and base metals were determined by ICP–MS (Inductively Coupled Plasma-Mass Spectrometry) following an aqua regia digestion. The precision and accuracy of ICP–ES and ICP–MS was evaluated using international standards, the replicate sample and additional analysis of selected samples by XRF (Niton XL3t). The analytical quality is satisfactory (<10 % error) for all elements, except for the Na_2O, P_2O_5, Ni, and Sn. These elements should be interpreted with caution.

Scanning Electron Microscope/Energy Dispersive Spectroscopy (SEM/EDS) analyses of selected samples were carried out in a low vacuum mode using a scanning electron microscope JEOL JSM 6490LV, coupled with an Oxford INCA Energy dispersive spectrometer at an accelerating voltage of 20 kV and working distance of 10 mm. Uncoated samples were observed in the BSE (backscattered electron) mode. The qualitative chemical composition of particles was measured using an EDS point X-ray microanalysis with an acquisition time of 10–30 s.

4 Results and discussion

4.1 Mineralogical composition

XRD patterns show the presence of large amounts of quartz in all samples, clay minerals dominated by illite and little chlorite in the majority, and a higher or lower amount of K-feldspar in some of them (Table 1).

Bulk XRD analysis revealed relatively low and broad reflections of clay minerals. Samples Iz14 and Iz20 consist of nearly pure K-feldspar with a probable minor content of quartz and clay minerals.

The presence of K-feldspar in the samples could confirm the idea of pyroclastic material (Alvaro and Bauluz 2008). The Jurassic evolution of the Neotethys is also associated with felsic magmatism (i.e. the Lemeš section) and the observed K-feldspar could be a consequence of such an event (Blaževković Smojić et al. 2009; Mikes et al. 2009). In contrast to the bentonites from the Lemeš section (Braun 1991), montmorillonite, which is typically of volcanic origin, was not found in any of the samples.

4.2 Geochemical composition

The origin of shale material could have been volcanogenic or terrigenous. The geochemical compositions of the samples (Table 2) reveal their true origin.

4.2.1 Volcanic versus terrigenous material

Besides the mineral composition of the samples, the K_2O content in the pure K-feldspar samples Iz14 and Iz20 is far too high for any igneous rock. Further, the Al_2O_3 content in samples Iz11, Iz13 and Iz15 speaks more in favour of shale than tuff.

In a discrimination diagram based on the contents of first-row transition metals and immobile elements (Andreozzi et al. 1997; Di Leo et al. 2002a, b), all of the Izvir samples are classified in the field of terrigenous sediments, with the exception of both K-feldspar-rich samples and the chert sample which are plotted outside of any field (Fig. 4).

The comparison of Izvir sediments relative to Post-Achaean Australian Shale–PAAS (Taylor and McLennan 1985), calculated in accordance with the recommendations of Hassan et al. (1999) and Di Leo et al. (2002a), shows that all three samples from the base of section (Iz11, Iz12 and Iz13) and one from the middle part (Iz17) are slightly depleted in Fe, Ca, Na, Mn, Co, Ba, Zn, and enriched in REE. Samples Iz15 and Iz19 show REE and Mn enrichment. K-feldspar-rich samples Iz14 and Iz20 differ from others in their high K content and less pronounced REE enrichment. In the diagrams K_2O, TiO_2, Cr and V versus Al_2O_3 (Fig. 5), all samples rich in clay minerals are close to PAAS values, supporting the terrigenous origin of the material. The chert samples show a silica dilution effect and the K-feldspar-rich samples a deviation from the trend.

Successions of interstratified chert and clay can be deposited in a variety of settings, ranging from a shelf to a mid-ocean ridge (Murray 1994). In his $100 \times Fe_2O_3/SiO_2$ versus $100 \times Al_2O_3/SiO_2$ and $Fe_2O_3/(100-SiO_2)$ versus $Al_2O_3/(100-SiO_2)$ diagram, Izvir cherts and shale samples plot in the area of continental margin depositional sites (Fig. 6). Also in the Fe_2O_3/TiO_2 versus $Al_2O_3/(Al_2O_3 + Fe_2O_3)$ diagram proposed by Girty et al. (1996) the Izvir

Table 2 Chemical composition of the Izvir shales and cherts (major elements in %, trace elements in ppm (mg/kg), *Ce/Ce** cerium anomaly)

	SiO_2	TiO_2	Al_2O_3	Fe_2O_3	MnO	MgO	CaO	Na_2O	K_2O	P_2O_5	LOI	C
Iz11	59.32	1.00	20.53	1.65	0.01	2.34	0.91	0.09	5.81	0.56	7.50	0.02
Iz12	61.35	0.91	16.90	7.83	0.01	0.93	0.39	0.15	2.62	0.20	8.40	0.05
Iz13	60.96	0.89	19.55	2.01	0.01	2.02	0.42	0.12	4.43	0.22	9.10	0.05
Iz14	60.53	0.75	17.04	4.15	0.03	0.22	0.07	0.12	14.40	0.16	2.50	0.02
Iz15	51.37	0.62	20.57	7.57	0.31	1.69	0.48	0.10	4.61	0.37	12.00	0.09
Iz16	91.55	0.11	3.11	1.39	0.17	0.31	0.11	0.08	0.64	0.07	2.30	0.05
Iz17	62.25	0.73	16.88	2.95	0.01	2.25	0.37	0.09	6.68	0.30	7.10	0.04
Iz18	96.26	0.04	1.00	0.43	0.03	0.12	0.07	0.05	0.40	0.06	1.10	0.03
Iz19	67.78	0.52	13.53	3.55	0.55	1.78	0.21	0.09	4.34	0.12	7.30	0.09
Iz20	58.80	0.68	18.90	1.67	0.02	1.99	0.20	0.09	11.13	0.06	6.20	0.05

	As	Cr	Ba	Co	Cs	Cu	Ga	Hf	Mo	Nb	Ni	Pb
Iz11	1.7	171	285	13.0	23.7	23.8	27.3	6.0	<0.1	21.0	56.0	11.3
Iz12	34.1	157	326	19.4	22.6	133.5	23.4	5.2	0.9	18.2	141.0	39.7
Iz13	2.5	137	291	9.5	27.9	35.2	22.4	5.4	<0.1	18.4	39.0	18.7
Iz14	14.2	5	42	15.3	1.0	67.7	8.1	4.2	0.4	5.6	72.0	52.4
Iz15	18.9	130	248	26.3	30.5	76.4	22.7	3.9	0.9	10.4	220.0	54.2
Iz16	6.2	34	65	5.6	3.4	17.1	3.9	0.6	0.2	1.9	39.0	14.6
Iz17	4.1	103	188	18.8	17.4	124.3	16.9	4.2	<0.1	13.2	82.0	44.7
Iz18	3.2	41	26	57.6	0.7	18.0	0.9	0.3	<0.1	0.7	28.0	5.8
Iz19	8.2	89	197	33.0	19.2	116.8	18.1	3.4	0.5	9.4	110.0	89.8
Iz20	5.7	55	84	10.9	10.9	95.5	15.7	7.8	<0.1	10.6	67.0	30.0

	Rb	Sc	Sr	Ta	Th	Tl	U	V	W	Y	Zn	Zr
Iz11	191.3	29	58.5	1.5	31.7	0.1	7.7	212	4.5	117.8	31	185.8
Iz12	160.1	19	49.9	1.3	14.3	0.2	3.5	175	4.4	69.2	191	174.7
Iz13	176.2	22	55.7	1.2	27.6	0.2	6.6	157	4.4	135.6	56	169.3
Iz14	74.8	13	12.5	0.5	4.5	0.1	6.3	49	2.7	28.1	119	104.3
Iz15	146.3	30	66.6	0.8	17.4	0.5	4.5	151	2.9	179.5	146	118.8
Iz16	26.4	7	12.5	0.1	3.3	0.2	1.1	26	0.4	31.3	32	19.8
Iz17	133.1	21	25.3	0.9	17.6	0.2	4.3	155	3.3	690.7	87	138.9
Iz18	8.5	3	8.6	0.4	1.1	0.1	0.5	5	367.4	17.2	16	8.9
Iz19	119.5	24	25.5	0.7	14.3	0.3	4.0	111	2.7	151.6	106	118.6
Iz20	110.0	16	10.5	1.4	19.8	0.1	6.2	84	2.4	103.6	73	187.2

	La	Ce	Pr	Nd	Sm	Eu	Gd	Tb	Dy	Ho	Er	Tm	Yb	Lu	Ce/Ce*
Iz11	116.1	127.7	28.2	130.4	24.9	5.7	20.5	2.7	14.8	2.9	8.0	1.1	6.1	0.9	0.57
Iz12	72.8	90.7	16.4	70.4	14.0	2.9	11.9	1.7	10.1	2.0	5.5	0.8	4.6	0.7	0.67
Iz13	135.0	193.4	41.3	193.1	37.3	7.6	28.8	3.6	18.6	3.4	8.3	1.1	6.5	0.9	0.66
Iz14	16.1	14.4	3.8	17.1	4.0	0.8	3.5	0.6	4.0	0.8	2.4	0.4	2.5	0.4	0.47
Iz15	173.3	121.6	36.2	165.3	32.2	7.0	29.8	4.1	23.6	4.7	12.4	1.7	10.2	1.4	0.39
Iz16	29.4	35.3	6.2	26.3	5.1	1.2	4.5	0.7	3.9	0.8	2.4	0.3	1.7	0.3	0.67
Iz17	243.9	121.2	57.9	272.8	57.0	13.3	70.8	10.2	62.5	13.7	37.2	4.6	23.9	3.8	0.26
Iz18	16.6	11.7	3.0	13.2	2.3	0.5	2.5	0.3	1.8	0.4	1.0	0.1	0.7	0.1	0.42
Iz19	143.0	150.7	28.5	125.9	23.7	5.1	21.9	3.0	18.0	3.9	10.4	1.5	8.8	1.3	0.60
Iz20	63.7	24.7	12.0	52.4	10.0	2.3	11.2	1.7	10.3	2.3	6.7	0.9	5.0	0.8	0.23

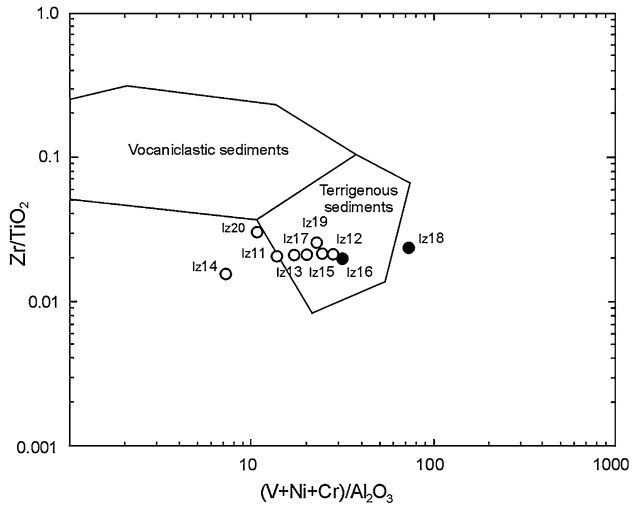

Fig. 4 Discrimination diagram for the volcanic versus terrigenous origin of material (Andreozzi et al. 1997). Symbols: *empty circles* shales, *full circles* chert

sediments plot in the area of the continental margin and old continental crust provenance (Fig. 7). The high values (min = 0.69, max = 0.93, average = 0.82) of parameter $D^* = Al_2O_3/(Al_2O_3 + MnO + FeO_{tot})$ proposed by Machhour et al. (1994) are in accordance with terrigenous material of a continental crust provenance. The MnO/TiO_2 ratio in shales is much lower than 0.5 and typical of a continental shelf, continental slope, marginal seas, or areas around a basaltic island (Shimizu et al. 2001).

According to the MnO/Al_2O_3 ratio, the sedimentation rate of the Izvir cherts was slow (2–4 m/Myr) and much faster (30 m/Myr) for interbedded shales. The different deposition rates could be interpreted as double accumulation, as suggested by Iijima et al. (1985). The chert accumulated at a relatively constant and slow rate, whereas terrigenous mud settled rapidly from periodical distal turbidity currents. The REE patterns of cherts and shales from Izvir are parallel. However, the cherts are somewhat less differentiated due to silica dilution. All of them have a pronounced negative Ce anomaly (Table 2), which is in favour of a slow deposition. This may be interpreted as either a reduced terrigenous input or as an open-sea sedimentary environment (Taylor and McLennan 1985). In areas of a slow sedimentation rate, REE patterns of sediments reflect the chemistry of the overlying water column, whereas REE in sediments deposited in areas of a relatively high sedimentation rate reflect more the average composition of source rocks, because quick burial limits seawater exposure time and restricts the capacity of the sediments to adsorb dissolved REE (Taylor and McLennan 1985). Izvir shales were deposited in the open-sea environment and consequently had been in contact with marine water long enough to acquire its REE pattern.

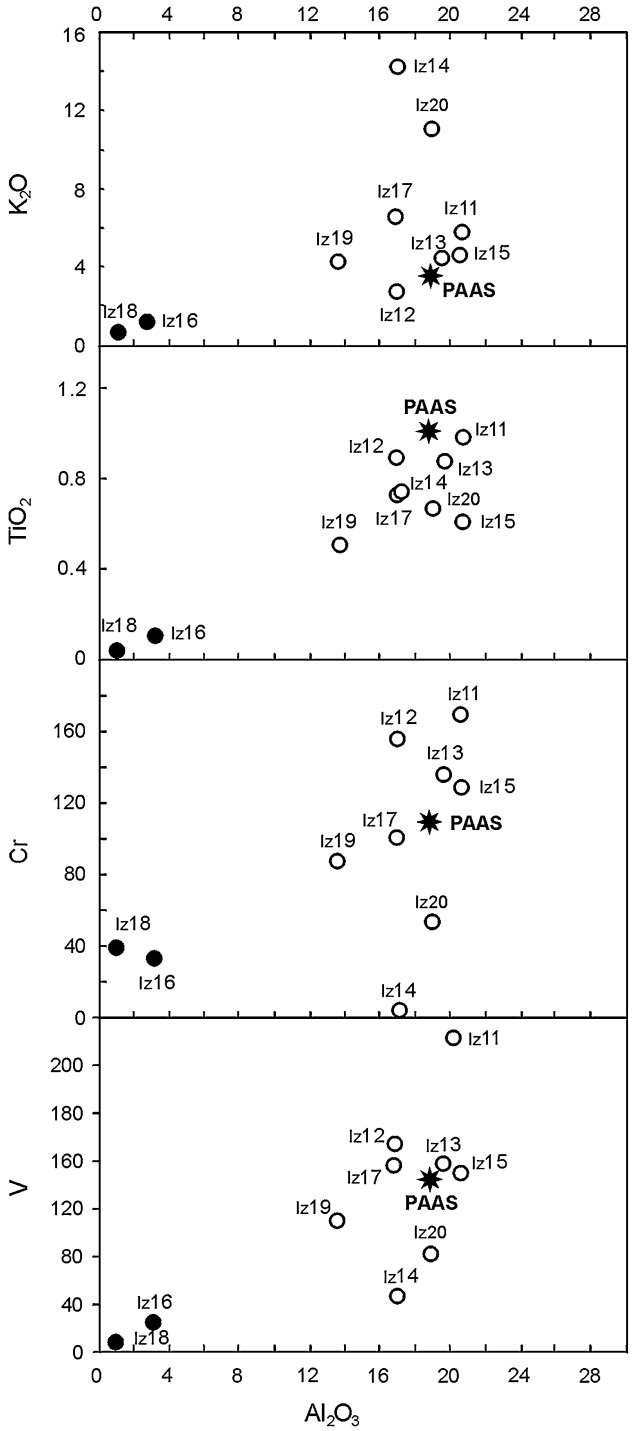

Fig. 5 K_2O, TiO_2, Cr and V versus Al_2O_3 diagram showing the close position to the post-Achaean Australian Shale (PAAS) values for shales, a silica dilution effect on the chert samples and a scatter from the trend for the K-feldspar-rich samples. *Symbols* same as for Fig. 4

4.2.2 *Hydrothermal influence*

As the Izvir interbedded material appears to have a terrigenous origin there should be a reason for the high potassium and subsequent K-feldspar content in some

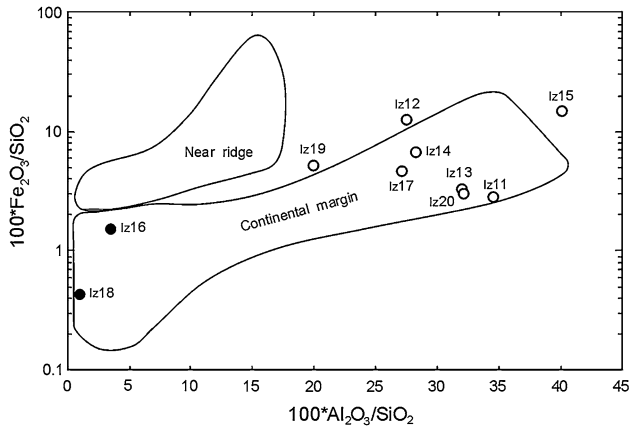

Fig. 6 $100 \times Fe_2O_3/SiO_2$ versus $100 \times Al_2O_3/SiO_2$ diagram (Murray 1994) of the Izvir sedimentary rocks. *Symbols* same as for Fig. 4

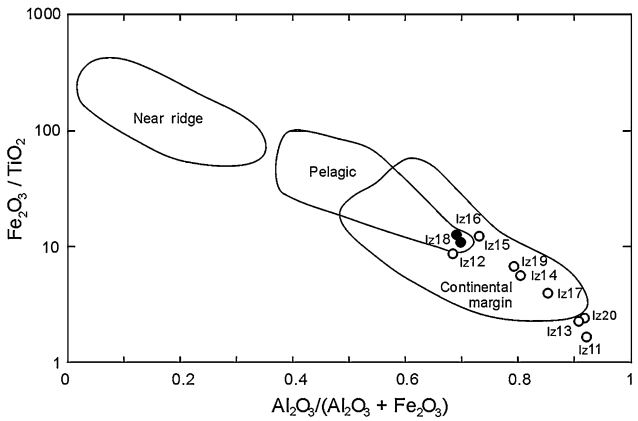

Fig. 7 Fe_2O_3/TiO_2 versus $Al_2O_3/(Al_2O_3 + Fe_2O_3)$ diagram (Girty et al. 1996) of the Izvir sedimentary rocks. *Symbols* same as Fig. 4

samples. One possibility could be enrichment by hydrothermal solutions (Di Leo et al. 2002a; Stefansson and Arnorsson 2000). In that case, some other elements, i.e. MnO, Cr and V, should also be elevated in comparison to the PAAS values (Barbera et al. 2006). Also the MnO/TiO_2 and Fe_2O_3 ratios should be enhanced (Yamamoto et al. 1986) and the Ba content high (Kyte et al. 1993). None of these features are observed in the Izvir samples. The non-hydrothermal origin is also corroborated by the Boström (1973) Fe_2O_3/TiO_2 versus $Al_2O_3/(Al_2O_3 + Fe_2O_3 + MnO)$ diagram (Fig. 8) in which samples are scattered, but plot near terrigenous or basaltic material.

Further, the high Al/(Al + Fe + Mn) ratio (average 0.8), used by Boström and Peterson (1969) as a measure of the hydrothermal contribution to sediments indicates biogenic hemipelagic cherts (Yamamoto et al. 1986). In the ternary Al–Fe–Mn diagram (Fig. 9) of Adachi et al. (1986), the samples plot in the non-hydrothermal area and even outside this field, closer to the Al apex.

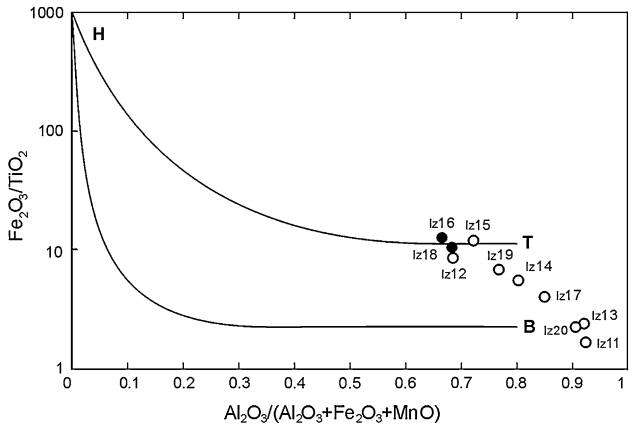

Fig. 8 Boström (1973) Fe_2O_3/TiO_2 versus $Al_2O_3/(Al_2O_3 + Fe_2O_3 + MnO)$ diagram; the analysed samples are close to terrigenous (*T*) or basaltic (*B*) material and far from a hydrothermal (*H*) end-member. *Symbols* same as for Fig. 4

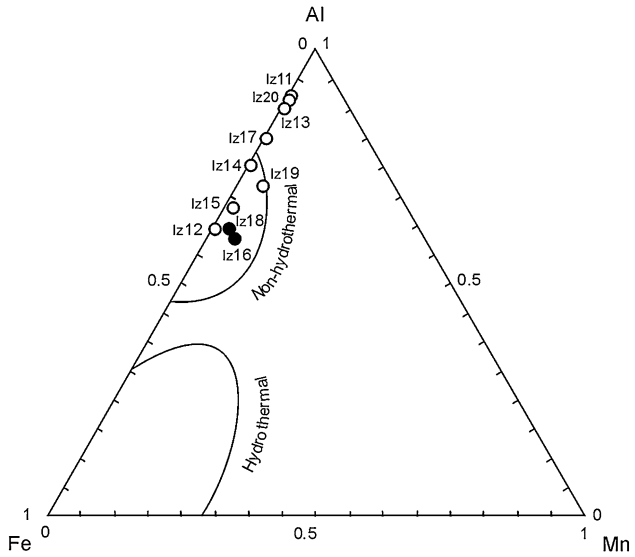

Fig. 9 Al–Fe–Mn diagram (Adachi et al. 1986) showing the non-hydrothermal character of the Izvir samples. *Symbols* same as for Fig. 4

4.2.3 Weathering

All of the samples except the two consisting of nearly pure K-feldspar (Iz14 and Iz20) have K_2O/Al_2O_3 values of less than 0.4, suggesting minimal alkali feldspar in the original rock (Cox et al. 1995). As volcanic and hydrothermal effects may be ruled out, the question arises as to whether just intense weathering and/or diagenetic changes could have affected the initial muddy sediments and caused the K-feldspar growth.

The degree and intensity of the chemical alteration of the earth materials are reflected in the chemical index of alteration $CIA = Al_2O_3/(Al_2O_3 + Na_2O + CaO + K_2O) \times 100$

(Nesbitt and Young 1982). The average CIA value of the Izvir interbeds is 68.8 (min = 52 for sample Iz14 and max = 82 for sample Iz12), which is characteristic of unweathered to slightly weathered detritus (Bahlburg and Dobrzinski 2009). The observed values are not very likely for such fine-grained and clay-rich material as the Izvir samples. In addition, the values of the chemical index of weathering (CIW = Al_2O_3/(Al_2O_3 + Na_2O + CaO)× 100; Harnois 1988), where no potash is included in the calculation, range from around 92 (sample Iz11) to 98 (sample Iz14), with an average value of 95.7, indicating intense and prolonged weathering (Barbera et al. 2006) and could support the interpretation that the material was already weathered to clay minerals when deposited between the chert beds. In addition, the index of compositional variability (ICV = (Fe_2O_3 + K_2O + Na_2O + CaO + MgO + TiO_2)/Al_2O_3; Cox et al. 1995) with values from 0.5 (Iz13) to 1.16 (Iz14) suggests that the material is generally compositionally mature (Barbera et al. 2006). The Zr/Sc versus Th/Sc diagram of McLennan et al. (1993) demonstrates that all Izvir sedimentary rocks have an upper crustal composition (Fig. 10) and were only slightly affected by recycling as the Zr/Sc ratio is low (Bahlburg and Dobrzinski 2009).

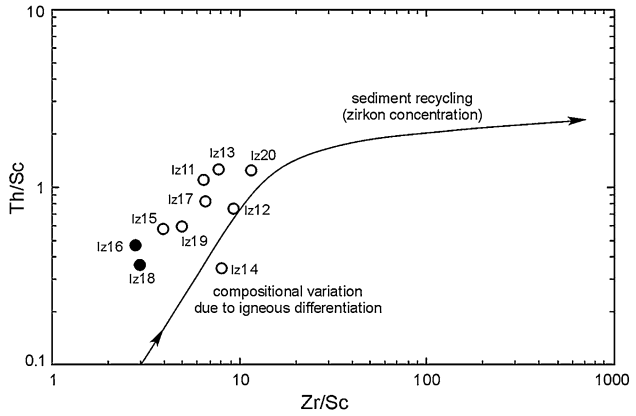

Fig. 10 Zr/Sc versus Th/Sc diagram (McLennan et al. 1993). *Symbols* same as for Fig. 4

Presumably, the majority of sedimented material was kaolinite with some additional terrigenous muscovite. For comparison, in the Dinarides, Ilic et al. (2005) report terrigenous white micas in graywackes of the Middle to Upper Jurassic mélange, suggesting the erosion of medium to deep crustal levels of the Variscan orogen. If the source material for the interbeds is weathered continental crust, the observed chemical and mineralogical compositions should follow the bulk compositional weathering trends predicted by Nesbitt and Young (1984). In the A–CN–K diagram the calculated weathering path should be directed towards kaolinite through the smectite or muscovite fields. In Fig. 11, only sample Iz12 lies somewhat closer to the kaolinite field. Other Izvir samples plot in the K_2O-rich area in the illite or the muscovite fields, some of them even in the pure K-feldspar field, which is not in accordance with predicted intense granite weathering. Further, the weathering trends of rocks with an intermediate to basic composition in the A–CNK–FM space (Fig. 11) should have compositional vectors directed away from biotite, hornblende and feldspar compositions (Nesbitt and Young 1989), whereas the Izvir samples show an irregular pattern. This erratic trend in the data again could be a result of diagenesis and/or metasomatism (Nesbitt and Young 1989; Fedo et al. 1995, 1997a, b; Cullers and Podkovyrov 2000).

4.2.4 *Diagenetic changes and K-metasomatism*

The question thus remains, whether the potassium-rich minerals—K-feldspar and muscovite/illite—in the Izvir

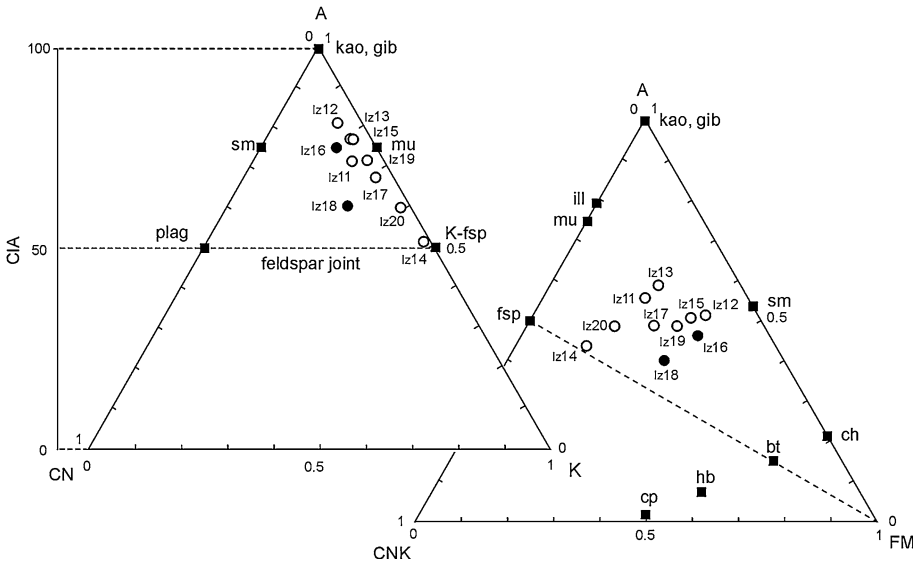

Fig. 11 A–CN–K and CNK–FM–A diagrams (Nesbitt and Young 1989) showing the Izvir samples' position out of the predicted weathering paths of andesite or granite. Their position corresponds to diagenetic potassium enrichment. Symbols: *A* Al_2O_3, *C* CaO, *N* Na_2O, *K* K_2O, *F* FeO_{total}, *M* MgO, samples same as in Fig. 4

samples have an entirely terrrigenous origin or, at least partly, a later, post-depositional, origin with sustained K_2O enrichment. It is difficult to differentiate terrigenous phases from authigenic ones (Fedo et al. 1997b), especially if an authigenic mineral overgrows a detritial core (Ali and Turner 1982). The additional problem of the terminology is that in the literature secondary K-feldspars have been described by a variety of genetic (largely overlapping) definitions such as authigenic, epigenetic, metasomatic, hydrothermal or secondary, but it can be accepted that all these K-feldspars were formed from low-temperature solutions during diagenesis (Arnaudov and Arnaudova 1997 and references therein).

K_2O values are quite enriched in the majority of Izvir samples and some of them (Iz14 and Iz20) even plot outside the upper crustal K_2O/Al_2O_3 ratio (Fig. 5). The high K_2O/Al_2O_3 ratio could be a consequence of potassium uptake during diagenesis (Plank and Langmuir 1998; Hutcheon et al. 2000).

Fedo et al. (1995) argue that K-metasomatism can involve the conversion of kaolinite into illite and/or conversion of plagioclase into K-feldspar. For the first possibility, the addition of potassium results in lower CIA values, but in the second one replacement by authigenic K-feldspar does not affect the CIA value. As the CIA values of the Izvir samples are obviously decreased, the authigenic replacement of plagioclase is ruled out and an aluminous clay conversion should be considered.

During early diagenesis the K^+/H^+ of the pore waters must decrease as the temperature increases to maintain an equilibrium with illite and kaolinite. During burial, illite would be produced at the expense of kaolinite. The amount of illite formed would be small if no K^+ were introduced by solutions from external sources. Illite is converted to K-feldspar as the temperature increases and K^+(aq) and pH tend to decrease (Nesbitt and Young 1989). With an increasing temperature, Mg^{2+} is consumed as well, and during diagenesis chlorite could form at the expense of kaolinite (Nesbitt and Young 1989). The present XRD results support various contents of K-feldspar (sample Iz14, CIA = 52), illite (sample Iz12, CIA = 82) and chlorite having been formed at the expense of kaolinite. An inspection of the samples with the SEM/EDS (Fig. 12) revealed up to 10 μm large euhedral K-feldspars, a feature in favour of their authigenic origin.

The source of potassium enrichment in the solution could be connected with the silicification of primary rocks to produce chert, as quartz precipitation releases K^+ to the solution (Nesbitt and Young 1989). Hearn and Sutter (1985) report the formation of authigenic K-feldspar in shallow-water limestones and dolostones at a low temperature through the reaction of brines with intercalated siliciclastic material. From field and microscopic

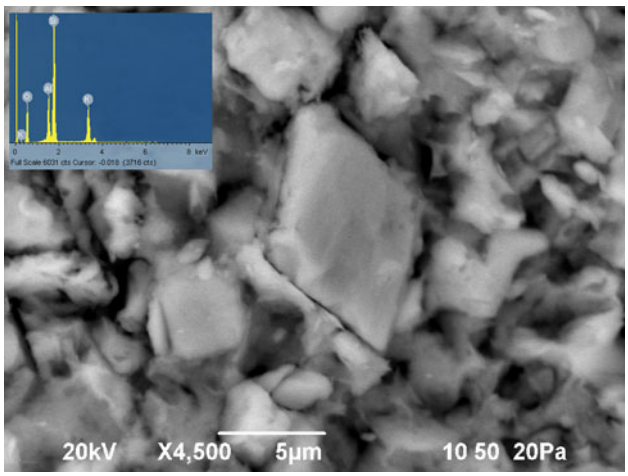

Fig. 12 The euhedral K-feldspars in sample Iz14 observed by SEM and EDS spectrum

observation it is obvious that the Izvir cherts formed as a consequence of the silicification of original siliceous carbonate beds. Such a process is possible in the mixing zone between meteoric and marine pore waters in coastal areas (Knauth 1979). Carbonate saturated meteoric waters may also become saturated with respect to opaline silica following the dissolution of biogenic siliceous shells. This explains why limited siliceous fossil remains are present. Upon the mixing with marine connate water, meteoric water immediately becomes undersaturated with respect to opal-A because of the low silica concentration in sea water (Hesse 1989). The simultaneous formation of K-feldspar by the reaction of brines with intercalated siliciclastic material is possible, with the migration of potassium from siliceous limestone—now chert beds—to interbedded clay. Kaolinite changed into illite/smectite and/or muscovite, and terrigenous muscovite into K-feldspar.

Field and microscopic observation of the Izvir beds supports the idea of siliceous limestone silicification. Geochemical data (Fig. 13) confirm that the cherts consist of organogenic silica while the shales contain predominantly terrigenous silica. The poorly preserved siliceous fossil remains support their diagenetic dissolution and reprecipitation causing limestone silification.

4.2.5 *Comparison with some other interbedded chert sequences*

A comparison of the geochemical characteristics of the Izvir interstratified material with *Scisti silicei* volcanoclastic beds (Di Leo et al. 2002b) using a *t* test shows statistically significant differences in the majority of elements. In the Italian volcaniclastic layers, Si, Na, Mn, and Ba are higher, and Al, Mg, K, Ti, Sc, Hf, Rb, Th, U, V, Cr and REE (except Ce) are lower than in the Izvir beds. Even

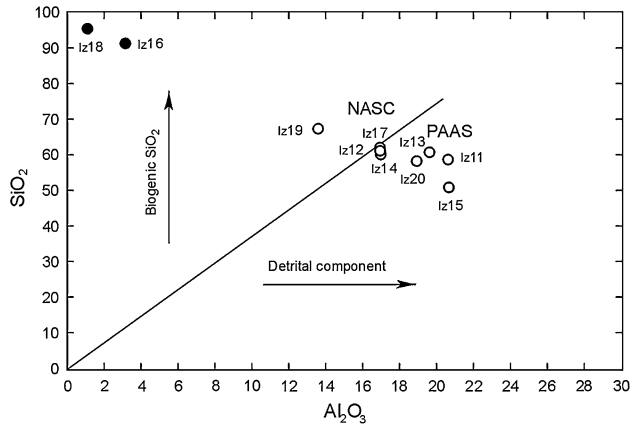

Fig. 13 Al_2O_3 versus SiO_2 diagram showing the biogenic origin of silica in cherts, and terrigenous origin in shales. *NASC* North American shale composite, *PAAS* post-Achaean Australian Shale. *Symbols* same as for Fig. 4

excluding the K-feldspar-rich samples (Iz14 and Iz20) from the analysis does not change the result. The origin and sedimentary environment of the Izvir and Lucanian Apennine deep-sea sediments are different.

For Jurassic continental-margin sequences in Croatia only geochemical data exist for Lemeš (Dalmatia) bentonites. Bentonites originated through the alteration of volcanic ash from acidic to intermediate lavas (Braun 1991). Late Jurassic bentonite beds are also known from the Southern Alps. Their mineralogical composition indicates that pyroclastics must have been connected to a distant source of original lava (Bernoulli and Peters 1970). However, the geochemical characteristics of material from both locations are different from the Izvir material.

In northern Croatia (for localities in this paragraph, see Fig. 1), data for radiolarian cherts of Jurassic and Triassic age show a wide spectrum of depositional environments and sources. Some Mt. Medvednica Jurassic cherts are consistent with an undifferentiated subduction-related magmatic arc characterised by the predominance of basic magmatic rocks as their average Al_2O_3/TiO_2 ratio is 8.14. However, a terrigenous origin from the accretionary prism comprising parts of MORB is not excluded (Halamić et al. 1999). Their Th/Sc ratio close to 0.5 also indicates an origin from magmatic or from an oceanic island arc (Halamić et al. 1999). The Mt. Medvednica cherts fall mostly in the field of continental margin sediments, although some of them are in the field of island arc provenance (Halamić et al. 2005). Halamić et al. (2001) interpret the negative Ce anomaly in continental-margin Triassic cherts at the Mt. Žumberak and Ivanščica localities as a consequence of a weaker terrigenous input because of the width of the disintegrated carbonate platform and consequently greater distance from the continent, or because of a topographically higher position and the bypass of fine terrigenous material.

The geochemical data for the Izvir samples are in accordance with deposition on a passive continental margin (Figs. 6, 7). These samples show no signature of arc-like clastic input and in this respect clearly differ from coeval cherts of the neighbouring Mt. Medvednica.

5 Conclusions

The Izvir shales interbedded with radiolarian cherts are laminated and very fine-grained. They are mainly composed of quartz and clay minerals dominated by illite, and probably some chlorite. In the majority of samples at least some K-feldspar is detected, while in some of them it is even the dominant component. Montmorillonite typical of a volcanic origin was not found. The major element contents show quite high SiO_2, Al_2O_3 and K_2O constituents, and low concentrations of other oxides. Different classification criteria imply that the shales have a terrigenous and not a volcanogenic origin.

The elevated potassium content and the presence of K-feldspar is not a consequence of hydrothermal enrichment since in the TiO_2, Cr and V versus Al_2O_3 diagrams the samples are close to the PAAS values, and MnO, Cr and V are not increased in comparison to PAAS. Furthermore, the elemental ratios plotted in different diagrams rule out a hydrothermal contribution.

The average chemical index of weathering (CIW) of 95.7 indicates an intense and prolonged source of weathering. Further, the index of compositional variability (ICV) suggest that the material is compositionally mature. In contrast, the average chemical index of alteration (CIA) of the Izvir interbeds is 68.8, which is characteristic of an unweathered to slightly weathered detritus. In the A–CN–K diagram, the Izvir samples plot on the K_2O rich side in the illite or muscovite field, some of them even in the pure K-feldspar field, which could be a result of diagenetic processes. As the CIA of the Izvir samples are obviously decreased, the authigenic replacement of plagioclase is ruled out and a diagenetic change of kaolinite into illite and chlorite, and muscovite into K-feldspar seems more probable.

From our observations, it is obvious that the Izvir cherts formed as a consequence of the silicification of originally more calcareous beds. The transformation occurred in the mixing zone between meteoric and marine pore waters. The siliceous, carbonate-saturated, meteoric waters became saturated with respect to opaline silica following the dissolution of biogenic siliceous shells. That is why few siliceous fossil remains are present. During mixing with marine connate water, the meteoric water became undersaturated with respect to opal-A because of the low silica concentration in the sea water. Simultaneously, K-feldspar was formed by the reaction of brines with intercalated

siliciclastic material by the migration of potassium from silicified carbonate beds to interlayered clay beds. The REE patterns of the Izvir samples show a pronounced negative Ce anomaly, which is characteristic of slowly accumulating sediments and prolonged contact with marine water. The MnO/Al_2O_3 ratio of the Izvir cherts supports their slow sedimentation rate but, on the contrary, it seems to be very fast for interbedded shales. The constantly slow accumulation of hemipelagic sediments rich in biogenic silica may have been periodically interrupted by the rapid sedimentation of terrigenous mud from distal turbidity currents.

The Izvir section was deposited on a Jurassic Tethyan passive continental margin. The original sediment was most probably biopelmicritic limestone rich in biogenic silica (radiolarians and sponge spicules). In some parts of the sequence siliceous carbonate beds were intercalated with muddy beds. The source material for the mud could be Variscan continental crust material with some larger terrigenous grains, i.e. muscovite. During diagenesis, the siliceous limestone was transformed to chert and potassium migrated and concentrated in the shales. Kaolinite was converted into illite and muscovite into K-feldspar.

Acknowledgments We thank Dr Josip Halamić and Dr Wilfried Winkler for the thorough revision of the manuscript. Their suggestions and comments have greatly improved the paper. Special thanks go to Dr Miloš Miler (Geological Survey of Slovenia–Geo-ZS) who enabled the SEM/EDS analyses. We are also very thankful to Dr Matej Dolenec (Department of Geology, University of Ljubljana) for performing the XRF analyses serving as an additional check of the chemical results. We thank Murray Bales for the language editing.

References

Adachi, M., Yamamoto, K., & Sugisaki, R. (1986). Hydrothermal chert and associated siliceous rocks from the northern Pacific: Their geological significance as indication of ocean ridge activity. *Sedimentary Geology, 47*, 125–148.

Ali, A. D., & Turner, P. (1982). Authigenic K-feldspar in the Bromsgrove Sandstone Formation (Triassic) of central England. *Journal of Sedimentary Research, 52*, 187–197.

Alvaro, J. J., & Bauluz, B. (2008). Feldspar concentration in lower Cambrian limestones of the Moroccan atlas: Pyroclastic vs. authigenic processes. *Journal of African Earth Sciences, 50*, 79–87.

Amodeo, F. (1999). Il Triassico terminale—Giurassico del Bacino Lagonegrese. Studi stratigrafici sugli Scisti Silicei della Basilicata (Italia meridionale). *Mémoires de Géologie, Lausanne,* 33, 1–121 (pls. 1–10).

Andreozzi, M., Dinelli, E., & Tateo, F. (1997). Geochemical and mineralogical criteria for the identification of ash layers in the stratigraphic framework of a foredeep; the Early Miocene Mt. Cervarola Sandstones, northern Italy. *Chemical Geology, 137*, 23–39.

Arnaudov, V., & Arnaudova, R. (1997). Authigenic K-feldspars as part of the adularias. Geochemistry. *Mineralogy and Petrology, 32*, 17–21.

Bahlburg, H., & Dobrzinski, N. (2009). A review of the chemical index of alteration (CIA) and its application to the study of neoproterozoic glacial deposits and climate transitions. In E. Arnaud, G. P. Halverson, & G. A. Shields-Zhou (Eds.), *The geological record of neoproterozoic glaciations. geological society, Memoir*, Vol. 36 (pp. 81–92). London: The Geological Society of London.

Baltuck, M. (1982). Provenance and distribution of Tethyan pelagic and hemipelagic sediments, Pindos Mountains, Greece. *Sedimentary Geology, 31*, 63–88.

Barbera, G., Mazzoleni, P., Critelli, S., Pappalardo, A., Lo Giudice, A., & Cirrincione, R. (2006). Provenance of shales and sedimentary history of the Monte Soro Unit, Sicily. *Periodico di Mineralogia, 75*, 313–330.

Barrett, T. J. (1981). Chemistry and mineralogy of Jurassic bedded chert overlying ophiolites in the North Apennines, Italy. *Chemical Geology, 34*, 289–317.

Baumgartner, P. O. (2013). Mesozoic radiolarites—accumulation as a function of sea surface fertility on Tethyan margins and in ocean basins. *Sedimentology, 60*, 292–318.

Baumgartner, P. O., Bartolini, A., Carter, E. S., Conti, M., Cortese, G., Danelian, T., De Wever, P., Dumitrica, P., Dumitrica-Jud, R., Goričan, Š., Guex, J., Hull, D. M., Kito, N., Marcucci, M., Matsuoka, A., Murchey, B., O'Dogherty, L., Savary, J., Vishnevskaya, V., Widz, D., & Yao, A. (1995a). Middle Jurassic to Early Cretaceous radiolarian biochronology of Tethys based on Unitary Associations. In P.O. Baumgartner, L. O'Dogherty, Š. Goričan, E. Urquhart, A. Pillevuit, & P. De Wever (Eds.), *Middle Jurassic to Lower Cretaceous Radiolaria of Tethys: Occurrences, systematics, Biochronology. Mémoires de Géologie (Lausanne)*, Vol. 23, (pp. 1013–1038). Lausanne: Université de Lausanne.

Baumgartner, P. O., Martire, L., Goričan, Š., O'Dogherty, L., Erba, E., & Pillevuit, A. (1995b). New middle and upper Jurassic radiolarian assemblages co-occurring with ammonites and nannofossils from the Southern Alps (Northern Italy). In P. O. Baumgartner, L. O'Dogherty, Š. Goričan, E. Urquhart, A. Pillevuit, & P. De Wever (Eds.), *Middle Jurassic to Lower Cretaceous Radiolaria of Tethys: Occurrences, systematics, biochronology. Mémoires de Géologie (Lausanne)*, Vol. 23 (pp. 737–749). Lausanne: Université de Lausanne.

Beccaro, P. (2006). Radiolarian biostratigraphy of middle-upper Jurassic pelagic siliceous successions of Western Sicily and the Southern Alps (Italy). *Mémoires de Géologie, Lausanne, 45*, 1–87 (pls. 1–12).

Bernoulli, D., & Peters, T. (1970). Traces of rhyolitic-trachytic volcanism in the upper Jurassic of the Southern Alps. *Eclogae Geologicae Helvetiae, 63*, 609–621.

Blažeković Smojić, S., Smajlović, J., Koch, G., Bulić, J., Trutin, M., Oreški, E., et al. (2009). Source potential and palynofacies of Late Jurassic » Lemeš facies « , Croatia. *Organic Geochemistry, 40*, 833–845.

Boström, K. (1973). The origin and fate of ferromanganoan active ridge sediments. *Stockholm Contributions in Geology, 27*, 147–243.

Boström, K., & Peterson, M. N. A. (1969). The origin of aluminium-poor ferromanganoan sediments in areas of high heat flow on the East Pacific Rise. *Marine Geology, 7*, 427–447.

Braun, K. (1991). Mineraloško-petrografske karakteristike i geneza ležišta bentonitskih glina Maovica, Gornje Jelenske, Bednje i Poljanske Luke (Mineralogical-petrographical characteristics and genesis of the bentonite deposits of Maovice, Gornja Jelenska, Bednja and Poljanska Luka). *Acta Geologica, 21*, 1–34.

Cox, R., Low, D. R., & Cullers, R. L. (1995). The influence of sediment recycling and basement composition on evolution of mudrock chemistry in the southwestern United States. *Geochimica Cosmochim Acta, 59*, 2919–2940.

Cullers, R. L., & Podkovyrov, V. N. (2000). Geochemistry of the Mesoproterozoic Lakhanda shales in southern Yakutia, Russia: implications for mineralogical and provenance control, and recycling. *Precambrian Research, 104*, 77–93.

Di Leo, P., Dinelli, E., Mongelli, G., & Schiattarella, M. (2002a). Geology and geochemistry of Jurassic pelagic sediments, Scisti silicei Formation, southern Apennines, Italy. *Sedimentary Geology, 150*, 229–246.

Di Leo, P., Giano, S. I., & Schiattarella, M. (2002b). Volcanoclastic layers in upper Triassic-Jurassic deep-sea sediments from the Lucanian Apennine, southern Italy: mineralogy, geochemistry, and palaeotectonic implications. *Periodico di Mineralogia, 71*, 49–63.

Fedo, C. M., Nesbitt, H. W., & Young, G. M. (1995). Unraveling the effects of potassium metasomatism in sedimentary rocks and paleosols, with implications for paleoweathering conditions and provenance. *Geology, 23*, 921–924.

Fedo, C. M., Young, G. M., & Nesbitt, H. W. (1997a). Paleoclimatic control on the composition of the Paleoproterozoic Serpent Formation, Huronian Supergroup, Canada: a greenhouse to icehouse transition. *Precambrian Research, 86*, 201–223.

Fedo, C. M., Young, G. M., Nesbitt, H. W., & Hanchar, J. M. (1997b). Potassic and sodic metasomatism in the Southern Province of the Canadian Shield: Evidence from the Paleoproterozoic Serpent Formation, Huronian Supergroup, Canada. *Precambrian Research, 84*, 17–36.

Girty, G. H., Ridge, D. L., Knaack, C., Johnson, D., & Al-Riyami, R. K. (1996). Provenance and depositional setting of Paleozoic chert and argillite, Sierra Nevada, California. *Journal of Sedimentary Research, 66*, 107–118.

Halamić, J., Goričan, Š., Slovenec, D., & Kolar-Jurkovšek, T. (1999). A Middle Jurassic Radiolarite-Clastic Succession from Medvednica Mt. (NW Croatia). *Geologia Croatica, 52*, 29–57.

Halamić, J., Marchig, V., & Goričan, Š. (2001). Geochemistry of Triassic radiolarian cherts in north-western Croatia. *Geologica Carpathica, 52*, 327–342.

Halamić, J., Marchig, V., & Goričan, Š. (2005). Jurassic radiolarian cherts in north-western Croatia: geochemistry, material provenance and depositional environment. *Geologica Carpathica, 56*, 123–136.

Harnois, L. (1988). The CIW index: A new chemical index of weathering. *Sedimentary Geology, 55*, 319–322.

Hassan, S., Ishiga, H., Roser, B. P., Dozen, K., & Naka, T. (1999). Geochemistry of Permian-Triassic shales in the Salt Range, Pakistan: implication for provenance and tectonism at the Gondwana margin. *Chemical Geology, 158*, 293–314.

Hearn, P. P., Jr, & Sutter, J. F. (1985). Authigenic potassium feldspar in Cambrian carbonates: evidence of Alleghanian brine migration. *Science, 228*, 1529–1531.

Hesse, R. (1989). Silica diagenesis: Origin of inorganic and replacement cherts. *Earth-Science Reviews, 26*, 253–284.

Hutcheon, I., Bloch, J., & Modus, S. (2000). Potassium enrichment in shale—fluid transport or provenance. *Journal of Geochemical Exploration, 69–70*, 17–22.

Iijima, A., Matsumoto, R., & Tada, R. (1985). Mechanism of sedimentation of rhythmically bedded cherts. *Sedimentary Geology, 41*, 221–233.

Ilic, A., Neubauer, F., & Handler, R. (2005). Late Plaeozoic-Mesozoic tectonics of the Dinarides revisited: Implications from 40Ar/39Ar dating of detritial white micas. *Geology, 33*, 233–236.

Knauth, L. P. (1979). A model for the origin of chert in limestone. *Geology, 776*, 274–277.

Kyte, F. T., Leinen, M., Heath, G. R., & Zhou, L. (1993). Elemental geochemistry of core LL44-GPC3 and a model for the Cenozoic sedimentation history of the central North Pacific. *Geochimica et Cosmochimica Acta, 57*, 1719–1740.

Machhour, L., Philip, J., & Oudin, J. L. (1994). Formation of Laminite deposits in anaerobic-dysaerobic marine environments. *Marine Geology, 117*, 287–302.

McLennan, S. M., Hemming, S., McDaniel, D. K., & Hanson, G. N. (1993). Geochemical approaches to sedimentation, provenance, and tectonics. In M. J. Johnsson, & A. Basu (Eds.), *Processes controlling the composition of clastic sediments, Special Paper Geological Society of America*, Vol. 284. (pp. 21–40). The Geological Society of America.

Mikes, T., Baresel, B., Kronz, A., Frei, D., Dunkl, I., Tolosana-Delgado, R., et al. (2009). Jurassic granitoid magmatism in the Dinaride Neotethys: geochronological constraints from detritial minerals. *Terra Nova, 21*, 495–506.

Mišič, M. (1998). *Clay minerals in Paleozoic and Mesosoic carbonate formations of Slovenia*. Ph.D dissertation, University of Ljubljana, Ljubljana, Slovenia, 164 pp [In Slovenian].

Moore, D. M., & Reynolds, R. C. (1997). *X-Ray diffraction and the identification and analysis of clay minerals*. Oxford: Oxford University Press.

Murray, R. W. (1994). Chemical criteria to identify the depositional environment of chert: General principles and applications. *Sedimentary Geology, 90*, 213–232.

Nesbitt, H. W., & Young, G. M. (1982). Early Proterozoic climates and plate motions inferred from major element chemistry of lutites. *Nature, 199*, 715–717.

Nesbitt, H. W., & Young, G. M. (1984). Prediction of some weathering trends of plutonic and volcanic rocks based on thermodynamic and kinetic considerations. *Geochimica et Cosmochimica Acta, 48*, 1532–1534.

Nesbitt, H. W., & Young, G. M. (1989). Formation and diagenesis of weathering profiles. *The Journal of Geology, 97*, 129–147.

Peh, Z., & Halamić, J. (2010). Discriminant function model as a tool for classification of stratigraphically undefined radiolarian cherts in ophiolite zones. *Journal of Geochemical Exploration, 107*, 30–38.

Placer, L. (1999). Contribution to the macrotectonic sudivision of the border region between Southern Alps and External Dinarides. *Geologija, 41*, 223–255.

Plank, T., & Langmuir, C. H. (1998). The chemical composition of subducting sediment and its consequences for the crust and mantle. *Chemical Geology, 145*, 325–394.

Rižnar, I. (2005). *Geology of the transitional area between outer and inner Dinarides, Eastern Slovenia*. Ph.D. dissertation, University of Zagreb, Zagreb, Croatia, 146 pp, app. 5 [In Slovenian].

Schmid, S. M., Bernoulli, D., Fügenschuh, B., Matenco, L., Schefer, S., Schuster, R., et al. (2008). The Alpine-Carpathian-Dinaridic orogenic system: correlation and evolution of tectonic units. *Swiss Journal of Geosciences, 101*, 139–183.

Schultz, L. G. (1964). Quantitative interpretation of minerlogical composition from X-ray and chemical data for the Pierre Shale. *US Geological Survey, Professional Papers 391-C*.

Shimizu, H., Kunimaru, T., Yoneda, S., & Adachi, M. (2001). Sources and depositional environments of some Permian and Triassic cherts: Significance of Rb-Sr and Sm-Nd isotopic and REE abundance data. *The Journal of Geology, 109*, 105–125.

Stefansson, A., & Arnorsson, S. (2000). Feldspar saturation state in natural waters. *Geochimica et Cosmochimica Acta, 64*, 2567–2584.

Taylor, S. R., & McLennan, S. M. (1985). *The continental crust: Its composition and evolution*. Oxford: Blackwell Scientific.

Velić, I., Tišljar, J., Vlahović, I., Velić, J., Koch, G., & Matičec, D. (2002). Paaeogeographic variability and depositional environments of the upper Jurassic carbonate rocks of Velika Kapela Mt. (Gorski Kotar Area, Adriatic Carbonate Platform, Croatia). *Geologia Croatica, 55*, 121–138.

Yamamoto, K., Sugisaki, R., & Arai, F. (1986). Chemical aspects of alteration of acidic tuffs and their application to siliceous deposits. *Chemical Geology, 55*, 61–76.